Journal of Harbin Engineering University
ISSN: 1006-7043

Vol 44 No. 8
August 2023

Fukui Functions, RDG, ELF, And LOL Analysis Of 2-Chloro-4,6-Diphenyl-1,3,5 Triazine Using DFT

Annu, B. S. Yadav[1], Jayant Teotia[2*]

[1,2*]Molecular Spectroscopy and Biophysics Laboratory, Department of Physics, Deva Nagri College, Meerut-250002, Uttar Pradesh, India

***Corresponding Author:** jayant.phy@gmail.com

Abstract
In the present work, various computational tools have been used for the analysis of 2-Chloro-4,6-diphenyl-1,3,5 triazine (CDP-1,3,5T) with the help of density functional theory (DFT) using the B3LYP method at 6-311++G(d,p) and cc-pVDZ basis sets. The study of non-covalent interactions helped in analyzing reduced density gradient. The chemical reactivity and selectivity for a local reactivity site have been analyzed using Fukui functions. The topological characteristics such as the Localized Orbital Locator and the Electron Localisation Function of CDP-1,3,5T are studied using Multiwfn software.

Keywords: CDP-1,3,5T, RDG, Fukui, ELF-LOL

1. Introduction

Triazine is an organic compound having a variety of uses in the industrial and medicinal fields. A novel triazine (R_1-MOF), which acts as a flame retardant and suppresses the release of smoke, has been synthesized to lower the toxicity of epoxy resin that polluted the environment [1]. The addition of an electron-affluent ketone group to the triazine-based covalent organic frameworks results in the narrowing of the band gap due to the hike in ketone content and these covalent organic framework-based catalysts have great potential in enhancing the photocatalytic degradation of the organic pollutants [2]. The substituted triazine derivatives have been used to synthesize hetero-cycle in the form of intermediates and reagents [3]. A triazine-based microporous organic network (TMON) is an excellent environmental adsorbent because of its recyclability and large surface area. The contaminants such as nadifloxacin and flumequine are effectively adsorbed by highly adaptable and stable TMON [4]. The s-triazine derivatives are endowed with higher selectivity and efficacy in blocking mechanisms owing to which they act as epidermal growth factor kinase inhibitors, thymidine phosphorylase, and protein kinase paving the way for the medicines to fight against breast cancer and tumours [5–7]. The incorporation of nanoparticles of calcium citrate and biguanide-based synthesis substituted triazine derivatives exhibited anticancer activity [8].

Owing to various applications and utilities of the triazine compounds, the 2-Chloro-4,6-diphenyl-1,3,5 triazine (CDP-1,3,5T) molecule has been chosen for the computational investigations assisted by density functional theory (DFT) using B3LYP/6-311++G(d,p) and B3LYP/cc-pVDZ basis sets.

2. Computational Details

The computational investigations on CDP-1,3,5T have been carried out using different computational programs with the help of 6-311++G(d,p) and cc-pVDZ basis sets by employing B3LYP method assisted by the Gaussian 09W [9] and Gaussview 6 [10] program to obtain the optimized structure of the molecule. The local reactivity descriptors, Electron Localisation Function (ELF), Localized Orbital Locator (LOL), and Reduced Density Gradient (RDG) have been examined using Multiwfn [11] and VMD [12] programs.

3. Results and Discussion

3.1 Structural parameters and geometry of the molecule

The molecular geometry of the CDP-1,3,5T molecule is shown in Figure 1 and the structural parameters of the compound have been obtained using 6–311++G(d,p) and cc–pVDZ basis sets at B3LYP level as shown in Table 1. The C–C bond length in the two benzene rings lies between 1.390 Å–1.406 Å for 6–311++G(d,p) and cc–pVDZ basis sets. Apart from the benzene ring C–C bond length is 1.479 Å at 6–311++G(d,p) level and 1.481 Å at cc–pVDZ level. The C–H bond length lies within 1.082 Å–1.084 Å and 1089 Å–1092 Å at 6–311++G(d,p) and cc–pVDZ levels respectively. The N–C bond length of the triazine ring of the CDP-1,3,5T molecule lies within 1.313 Å–1.348 Å and 1.323 Å–1.351 Å at 6–311++G(d,p) and cc–pVDZ levels respectively. C–Cl bond length 1.753 Å at 6–311++G(d,p) level and 1.756 Å at cc–pVDZ level. In the triazine ring C–N–C and N–C–Cl bond angles lie within 114.4°–116.5° at 6–311++G(d,p) level and 114°–116.2° at cc–pVDZ level. The N–C–C bond angles are of the order of 118° for both basis sets. The N–C–N bond angles can be visualized between 123.7°–127.6° at 6–311++G(d,p)

level and 124°–128° at cc–pVDZ level. The N–C–C and C–C–C bond angles lie between 119°–121° for both the basis sets. The computed values of bond lengths and bond angles of the CDP-1,3,5T molecule are almost the same for 6–311++G(d,p) and cc–pVDZ basis sets.

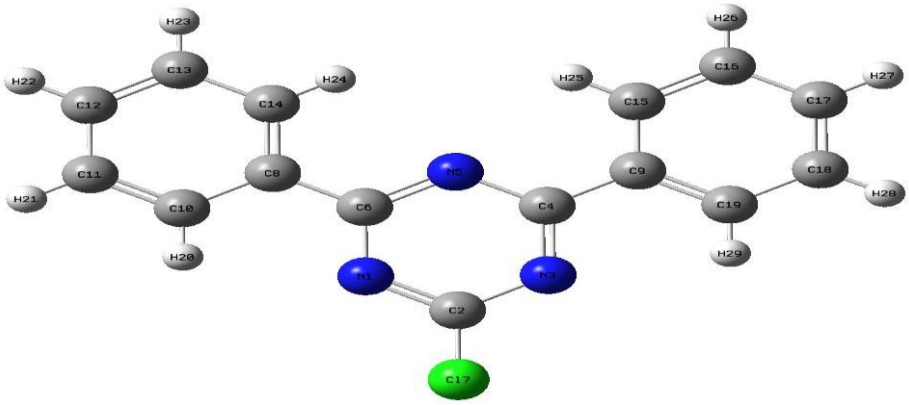

Figure 1. Structure of the CDP-1,3,5T molecule.

Table 1. Computed optimized structural parameters of CDP-1,3,5T molecule.

Bond Length (Å)	B3LYP/ 6–311G++(d, p)	B3LYP/ cc–pVDZ	Bond Angle (°)	B3LYP/ 6–311G++(d, p)	B3LYP/ cc–pVDZ
N1–C2	1.318	1.323	C2–N1–C6	114.3	114.0
N1–C6	1.347	1.351	N1–C2–N3	127.6	128.0
C2–N3	1.318	1.323	N1–C2–Cl 7	116.2	116.1
C2–Cl 7	1.753	1.756	N3–C2–Cl 7	116.2	116.1
N3–C4	1.348	1.351	C2–N3–C4	114.3	114.0
C4–N5	1.338	1.342	N3–C4–N5	123.7	124.0
C4–C9	1.479	1.481	N3–C4–C9	117.6	117.4
N5–C6	1.338	1.342	N5–C4–C9	118.7	118.6
C6–C8	1.479	1.481	C4–N5–C6	116.5	116.2
C8–C10	1.402	1.406	N1–C6–N5	123.7	124.0
C8–C14	1.402	1.406	N1–C6–C8	117.6	117.4
C9–C15	1.402	1.406	N5–C6–C8	118.7	118.6
C9–C19	1.402	1.406	C6–C8–C10	120.2	120.1
C10–C11	1.390	1.394	C6–C8–C14	120.4	120.5
C10–H20	1.082	1.090	C10–C8–C14	119.4	119.4
C11–C12	1.395	1.399	C4–C9–C15	120.4	120.5
C11–H21	1.084	1.092	C4–C9–C19	120.2	120.1
C12–C13	1.395	1.399	C15–C9–C19	119.4	119.4
C12–H22	1.084	1.092	C8–C10–C11	120.2	120.2
C13–C14	1.390	1.394	C8–C10–H20	119.0	119.0
C13–H23	1.084	1.092	C11–C10–H20	120.8	121.0
C14–H24	1.082	1.089	C10–C11–C12	120.2	120.1
C15–C16	1.390	1.394	C10–C11–H21	119.8	120.0
C15–H25	1.082	1.089	C12–C11–H21	120.1	120.1
C16–C17	1.395	1.399	C11–C12–C13	120.0	120.0
C16–H26	1.084	1.092	C11–C12–H22	120.0	120.0
C17–C18	1.395	1.399	C13–C12–H22	120.0	120.0
C17–H27	1.084	1.092	C12–C13–C14	120.1	120.1
C18–C19	1.390	1.394	C12–C13–H23	120.1	120.1
C18–H28	1.084	1.092	C14–C13–H23	120.0	120.0
C19–H29	1.082	1.090	C8–C14–C13	120.2	120.2
			C8–C14–H24	119.0	119.0
			C13–C14–H24	120.7	121.0
			C9–C15–C16	120.2	120.0
			C9–C15–H25	119.0	119.0
			C16–C15–H25	120.7	121.0
			C15–C16–C17	120.1	120.1
			C15–C16–H26	120.0	120.0
			C17–C16–H26	120.1	120.1
			C16–C17–C18	120.0	120.0
			C16–C17–H27	120.0	120.0
			C18–C17–H27	120.0	120.0

C17–C18–C19	120.2	120.1
C17–C18–H28	120.1	120.1
C19–C18–H28	120.0	120.0
C9–C19–C18	120.2	120.2
C9–C19–H29	119.0	119.0
C18–C19–H29	121.0	121.0

The molecular geometry of the CDP-1,3,5T molecule is shown in Figure 1 and the structural parameters of the compound have been obtained using 6–311++G(d,p) and cc–pVDZ basis sets at B3LYP level as shown in Table 1. The C–C bond length in the two benzene rings lies between 1.390 Å–1.406 Å for 6–311++G(d,p) and cc–pVDZ basis sets. Apart from the benzene ring C–C bond length is 1.479 Å at 6–311++G(d,p) level and 1.481 Å at cc–pVDZ level. The C–H bond length lies within 1.082 Å–1.084 Å and 1089 Å–1092 Å at 6–311++G(d,p) and cc–pVDZ levels respectively. The N–C bond length of the triazine ring of the CDP-1,3,5T molecule lies within 1.313 Å–1.348 Å and 1.323 Å–1.351 Å at 6–311++G(d,p) and cc–pVDZ levels respectively. C–Cl bond length 1.753 Å at 6–311++G(d,p) level and 1.756 Å at cc–pVDZ level. In the triazine ring C–N–C and N–C–Cl bond angles lie within 114.4°–116.5° at 6–311++G(d,p) level and 114°–116.2° at cc–pVDZ level. The N–C–C bond angles are of the order of 118° for both basis sets. The N–C–N bond angles can be visualized between 123.7°–127.6° at 6–311++G(d,p) level and 124°–128° at cc–pVDZ level. The N–C–C and C–C–C bond angles lie between 119°–121° for both the basis sets. The computed values of bond lengths and bond angles of the CDP-1,3,5T molecule are almost the same for 6–311++G(d,p) and cc–pVDZ basis sets.

3.2 Local Reactivity Descriptors

The local reactivity descriptors such as Fukui functions are used to estimate the chemical reactivity and selectivity sites in a molecule based on electrophilicity and nucleophilicity [13].
The condensed dual descriptor $\Delta f(r)$ is given by
$\Delta f(r)= [f^{+}-f^{-}]$

The condensed Fukui functions for different reactivity sites are listed below:
For the nucleophilic attack ($\Delta f(r) >0$), $f_j^{+} = q_j(N+1)-q_j(N)$ [14]
For an electrophilic attack ($\Delta f(r)<0$), $f_j^{-} = q_j(N)-q_j(N-1)$
For radical attack, $f_j^{0}=1/2[q_j(N+1)-q_j(N-1)]$

where q_j is the charge on the atom at the jth level; N, N+1, and N−1 are the number of electrons in the neutral, anionic, and cationic states respectively [15].

If $\Delta f(r)>0$, the condition is conducive to the attack by a nucleophile while $\Delta f(r)<0$ is conducive to the attack by an electrophile. Multiwfn program [11] assisted in calculating the dual descriptors and Hirshfeld charges [q(N), q(N+1), q(N−1)] of the CDP-1,3,5T molecule as depicted in Table 2. C4 and C6 atoms have the most positive values (0.0589) which signifies that they are likely to be attacked by a nucleophile whereas C8 and C9 have the most negative values (−0.0405) hinting towards the attack by an electrophile. The negative value of the descriptors points toward the biological activity of the CDP-1,3,5T molecule which might bind with the proteins [16].

Table 2. Hirshfeld charges, condensed Fukui functions [f_j^{-}, f_j^{+}, f_j^{0}], and condensed dual descriptors $\Delta f(r)$ of CDP-1,3,5T {Units used below are "e" (elementary charge)}.

Atom	q(N)	q(N+1)	q(N−1)	f^{-}	f^{+}	f^{0}	CDD
1(N)	−0.1585	−0.2239	−0.139	0.0194	0.0654	0.0424	0.046
2(C)	0.1434	0.1139	0.1604	0.0171	0.0294	0.0232	0.0124
3(N)	−0.1585	−0.2239	−0.139	0.0194	0.0654	0.0424	0.046
4(C)	0.1323	0.0633	0.1425	0.0101	0.069	0.0396	0.0589
5(N)	−0.146	−0.1637	−0.104	0.042	0.0177	0.0298	−0.0243
6(C)	0.1323	0.0633	0.1425	0.0101	0.069	0.0396	0.0589
7(Cl)	−0.0506	−0.1329	0.0128	0.0633	0.0824	0.0729	0.019
8(C)	−0.0125	−0.0243	0.0397	0.0522	0.0118	0.032	−0.0405
9(C)	−0.0125	−0.0243	0.0397	0.0522	0.0118	0.032	−0.0405
10(C)	−0.0255	−0.0594	−0.0006	0.025	0.0339	0.0294	0.0089
11(C)	−0.0344	−0.0636	0.0249	0.0593	0.0292	0.0442	−0.0301
12(C)	−0.0254	−0.0815	0.0466	0.0719	0.0561	0.064	−0.0158
13(C)	−0.0358	−0.0666	−0.0068	0.0291	0.0308	0.0299	0.0017
14(C)	−0.0277	−0.0543	0.0187	0.0464	0.0267	0.0365	−0.0198
15(C)	−0.0277	−0.0543	0.0187	0.0464	0.0267	0.0365	−0.0197
16(C)	−0.0358	−0.0666	−0.0068	0.0291	0.0308	0.0299	0.0017
17(C)	−0.0254	−0.0815	0.0466	0.0719	0.0561	0.064	−0.0158
18(C)	−0.0344	−0.0636	0.0249	0.0593	0.0292	0.0442	−0.0301

19(C)	−0.0255	−0.0594	−0.0006	0.025	0.0339	0.0294	0.0089
20(H)	0.0412	0.021	0.0612	0.02	0.0201	0.0201	0.0001
21(H)	0.0448	0.0215	0.0752	0.0304	0.0233	0.0269	−0.0071
22(H)	0.0453	0.0133	0.0782	0.0329	0.032	0.0324	−0.0009
23(H)	0.0438	0.0207	0.068	0.0242	0.0231	0.0237	−0.0011
24(H)	0.0392	0.0256	0.0569	0.0177	0.0135	0.0156	−0.0041
25(H)	0.0392	0.0256	0.0569	0.0177	0.0135	0.0156	−0.0041
26(H)	0.0438	0.0207	0.068	0.0242	0.0231	0.0237	−0.0011
27(H)	0.0453	0.0133	0.0782	0.0329	0.032	0.0324	−0.0009
28(H)	0.0448	0.0215	0.0752	0.0304	0.0233	0.0269	−0.0071
29(H)	0.0412	0.021	0.0612	0.02	0.0201	0.0201	0.0001

3.3 Wave function Analysis: Electron Localisation Function (ELF) and Localized Orbital Locator (LOL)

The electronic wave function interpretation can be achieved using LOL and ELF surfaces. The repulsion theory given by Pauli plays a pivotal role in comprehending ELF. For the maximum value of Pauli's repulsion, the value of ELF is closer to one and if this value is minimum then ELF is equal to zero due to the difference in the kinetic energy [17]. The localized electron cloud can be studied with the help of LOL. The ELF and LOL surfaces of the CDP-1,3,5T molecule are shown in Figure 2 and Figure 3 respectively.

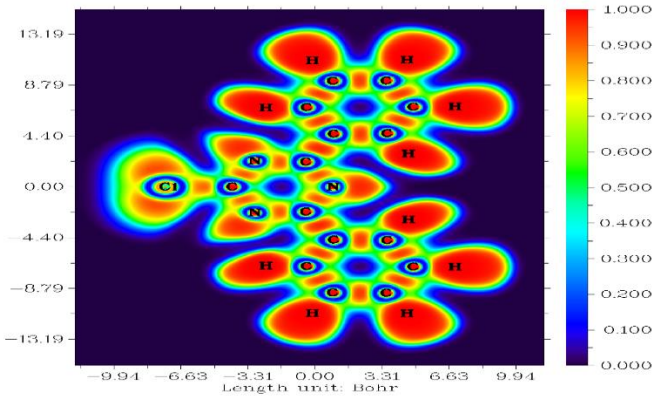

Figure 2. ELF surface of CDP-1,3,5T

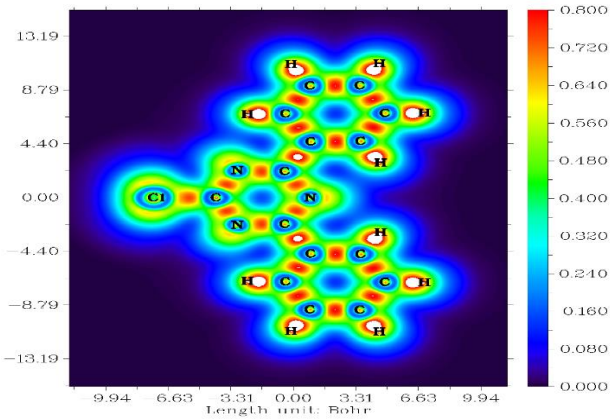

Figure 3. LOL surface of CDPT

The dark blue region of the CDP-1,3,5T molecule indicates the electronically depleted region inside the shells that can be visualized around nitrogen, carbon, and chlorine signifies lower values of ELF while the red colour implies high localized electrons and the presence of the nucleus of an atom on account of maximum Pauli repulsion leading to higher values of ELF as seen around the hydrogen atom [13,18]. In LOL, the blue colour encompassing carbon, chlorine, and nitrogen of the CDP-1,3,5T molecule indicates the presence of a depletion region of the electrons between inner and valence shells whereas the red colour around carbon-carbon, nitrogen-carbon, and chlorine-carbon suggests the prevalence of covalent regions. The high density of electrons around the hydrogen atoms is represented by white colour [19].

3.4 Reduced Density Gradient (RDG) Analysis

The non–covalent interactions dependent on electron density gradient ∇*ρ(r)* can be interpreted graphically with the help of reduced density gradient (RDG) *S(r)* [20,21] with the help of the following relation:

$$S(r) = \frac{|\nabla \rho(r)|}{2(3\pi)^{\frac{1}{3}}\rho(r)^{\frac{4}{3}}}$$

These interactions are characterized by low–density, weak, and low–reduced gradients that have a positive value of the Laplacian while for the covalent interactions, this value is negative [20,22].

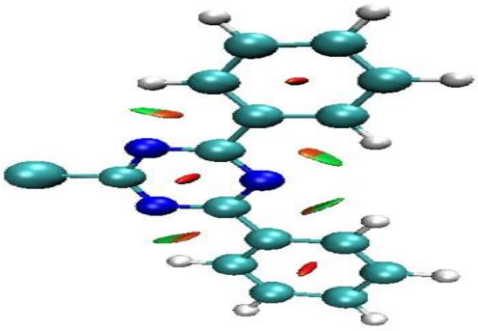

Figure 4. Isosurface of CDP-1,3,5T in three dimensions

The iso-surface and the scatter plot between the sign (λ_2) ρ and RDG of the CDP-1,3,5T molecule are shown in Figure 4 and Figure 5 respectively. If the value of the second derivative of the electron density of the Hessian matrix (λ_2) ρ is ≈ 0 then it implies weak interactive regions due to van der Waals forces and is shown in green. $\lambda_2 < 0$ signifies bonding and strong attractive interactions shown by the blue colour. $\lambda_2 > 0$ represents non–bonding and strong repulsive interactions paving the way for steric effect in rings as shown by the red colour.

In the CDP-1,3,5T molecule, the green-coloured area on the iso-surface around hydrogen represents van der Waals interactions. The red colour at the centre of the isosurface of the triazine and benzene rings signifies steric effect in the rings arising due to the strong repulsion and the corresponding RDG scatter plot lies in between 0.014–0.03 a.u.

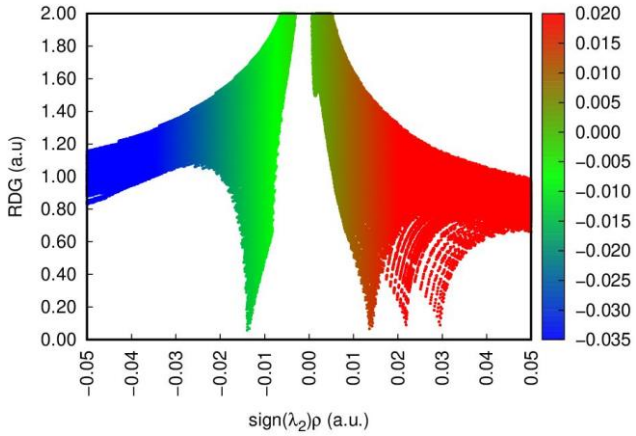

Figure 5. Reduced density gradient scatter plot of CDP-1,3,5T

4. Conclusion

The computational details of the CDP-1,3,5T molecule have been reported for the first time. The bond angle and the bond length have been calculated which matches with the literature. The ELF-LOL, RDG, and Fukui Indices confirmed that the compound is stable and chemically reactive. The reduced density gradient investigations of CDP-1,3,5T proved the steric effect in the triazine ring. Fukui indices study shows that the nitrogen atoms in the CDP-1,3,5T molecule are prone to electrophilic attack while the space surrounding the hydrogen and carbon atoms is attacked by the nucleophiles. Thus, it can be concluded that the CDP-1,3,5T molecule is a stable molecule having the potential to be used in the field of medicine.

References

1. G. Zhang, W. Wu, M. Yao, Z. Wu, Y. Jiao, H. Qu, Novel triazine-based metal-organic frameworks: synthesis and mulifunctional application of flame retardant, smoke suppression and toxic attenuation on EP, Mater. Des. 226 (2023) 1–8. https://doi.org/10.1016/j.matdes.2023.111664.
2. X. Li, L. Zhang, S. Niu, Z. Dong, C. Lyu, Quantitatively regulating the ketone structure of

triazine-based covalent organic frameworks for efficient visible-light photocatalytic degradation of organic pollutants: Tunable performance and mechanisms, J. Hazard. Mater. 444 (2023). https://doi.org/10.1016/J.JHAZMAT.2022.130366.

3. G. Giacomelli, A. Porcheddu, L. Luca, [1,3,5]-Triazine: A Versatile Heterocycle in Current Applications of Organic Chemistry, Curr. Org. Chem. 8 (2005) 1497–1519. https://doi.org/10.2174/1385272043369845.
4. Z. Zhao, S. Lin, Z. Yu, M. Su, B. Liang, S.X. Liang, X.H. Ju, Facile synthesis of triazine-based microporous organic network for high-efficient adsorption of flumequine and nadifloxacin: A comprehensive study on adsorption mechanisms and practical application potentials, Chemosphere. 315 (2023). https://doi.org/10.1016/J.CHEMOSPHERE.2022.137731.
5. N. Akram, A. Mansha, R. Premkumar, A.M. Franklin Benial, S. Asim, S.Z. Iqbal, H.S. Ali, Spectroscopic, quantum chemical and molecular docking studies on 2,4-dimethoxy-1,3,5-triazine: a potent inhibitor of protein kinase CK2 for the development of breast cancer drug, Mol. Simul. 46 (2020) 1340–1353. https://doi.org/10.1080/08927022.2020.1822526.
6. M.S. Raghu, C.B.P. Kumar, M.K. Prashanth, K.Y. Kumar, Novel 1,3,5-triazine-based pyrazole derivatives as potential antitumor agents and EFGR kinase inhibitors: synthesis, cytotoxicity, DNA binding, molecular docking and DFT studies, (2021) 13909–13924. https://doi.org/10.1039/d1nj02419a.
7. M. Manachou, Z. Gouid, Z. Almi, S. Belaidi, S. Boughdiri, M. Manachou, Z. Gouid, Z. Almi, S. Belaidi, S. Boughdiri, Pyrazolo[1,5-a][1,3,5]triazin-2-thioxo-4-ones derivatives as thymidine phosphorylase inhibitors : Structure , drug-like calculations and quantitative structure-activity relationships (QSAR) modeling To cite this version : HAL Id : hal-02974009, J. Mol. Struct. 1199 (2021) 22. https://doi.org/10.1016/j.molstruc.2019.127027.
8. M. Chalermnon, C. Sarocha, A. Sereemaspun, R. Rojanathanes, T. Khotavivattana, Biguanide-Based Synthesis of 1,3,5-Triazine Derivatives with Anticancer Activity and 1,3,5-Triazine Incorporated Calcium Citrate Nanoparticles, Molecules. 26 (2021) 1–14. https://doi.org/https://doi.org/10.3390/molecules26041028.
9. M.J. Frisch, G.W. Trucks, H.B. Schlegel, G.E. Scuseria, M.A. Robb, J.R. Cheeseman, G. Scalmani, V. Barone, B. Mennucci, G.A. Petersson, H. Nakatsuji, M. Caricato, X. Li, H.P. Hratchian, A.F. Izmaylov, J. Bloino, G. Zheng, J.L. Sonnenberg, M. Hada, M. Ehara, K. Toyota, R. Fukuda, J. Hasegawa, M. Ishida, T. Nakajima, Y. Honda, O. Kitao, H. Nakai, T. Vreven, J.A. Montgomery, J.E. Peralta, F. Ogliaro, M. Bearpark, J.J. Heyd, E. Brothers, K.N. Kudin, V.N. Staroverov, R. Kobayashi, J. Normand, K. Raghavachari, A. Rendell, J.C. Burant, S.S. Iyengar, J. Tomasi, M. Cossi, N. Rega, J.M. Millam, M. Klene, J.E. Knox, J.B. Cross, V. Bakken, C. Adamo, J. Jaramillo, R. Gomperts, R.E. Stratmann, O. Yazyev, A.J. Austin, R. Cammi, C. Pomelli, J.W. Ochterski, R.L. Martin, K. Morokuma, V.G. Zakrzewski, G.A. Voth, P. Salvador, J.J. Dannenberg, S. Dapprich, A.D. Daniels, Ö. Farkas, J.B. Foresman, J. V. Ortiz, J. Cioslowski, D.J. Fox, Gaussian09, Gaussian 09. (2009).
10. 2016. GaussView, Version 6, Dennington, Roy; Keith, Todd A.; Millam, John M. Semichem Inc., Shawnee Mission, KS, GaussView 6, Gaussian. (2016).
11. T. Lu, F. Chen, Multiwfn: A multifunctional wavefunction analyzer, J. Comput. Chem. 33 (2012) 580–592. https://doi.org/10.1002/jcc.22885.
12. W. Humphrey, A. Dalke, K. Schulten, VMD: Visual Molecular Dynamics, J. Mol. Graph. (1996).
13. S. Sevvanthi, S. Muthu, S. Aayisha, P. Ramesh, M. Raja, Spectroscopic (FT-IR, FT-Raman and UV-Vis), computational (ELF, LOL, NBO, HOMO-LUMO, Fukui, MEP) studies and molecular docking on benzodiazepine derivatives-heterocyclic organic arenes, Chem. Data Collect. 30 (2020) 100574. https://doi.org/10.1016/j.cdc.2020.100574.
14. J. Padmanabhan, R. Parthasarathi, M. Elango, V. Subramanian, B.S. Krishnamoorthy, S. Gutierrez-Oliva, A. Toro-Labbé, D.R. Roy, P.K. Chattaraj, Multiphilic descriptor for chemical reactivity and selectivity, J. Phys. Chem. A. 111 (2007) 9130–9138. https://doi.org/10.1021/jp0718909.
15. S. Saravanan, V. Balachandran, Quantum mechanical study and spectroscopic (FT-IR, FT-Raman, UV-Visible) study, potential energy surface scan, Fukui function analysis and HOMO-LUMO analysis of 3-tert-butyl-4-methoxyphenol by DFT methods, Spectrochim. Acta - Part A Mol. Biomol. Spectrosc. 130 (2014) 604–620. https://doi.org/10.1016/j.saa.2014.04.058.
16. A. Saral, P. Sudha, S. Muthu, A. Irfan, Computational, spectroscopic and molecular docking investigation on a bioactive anti-cancer drug: 2-Methyl-8-nitro quinoline, J. Mol. Struct. 1247 (2022) 131414. https://doi.org/10.1016/j.molstruc.2021.131414.
17. J. George, J.C. Prasana, S. Muthu, T.K. Kuruvilla, S. Sevanthi, R.S. Saji, Spectroscopic (FT-IR, FT Raman) and quantum mechanical study on N-(2,6-dimethylphenyl)-2-{4-[2-hydroxy-3-(2-methoxyphenoxy) propyl] piperazin-1-yl} acetamide, J. Mol. Struct. 1171 (2018) 268–278. https://doi.org/10.1016/j.molstruc.2018.05.106

.

18. R.S. Saji, J.C. Prasana, S. Muthu, J. George, T.K. Kuruvilla, B.R. Raajaraman, Spectroscopic and quantum computational study on naproxen sodium, Spectrochim. Acta - Part A Mol. Biomol. Spectrosc. 226 (2020) 117614. https://doi.org/10.1016/j.saa.2019.117614.
19. A. Saral, P. Sudha, S. Muthu, S. Sevvanthi, P. Sangeetha, S. Selvakumari, Vibrational spectroscopy, quantum computational and molecular docking studies on 2-chloroquinoline-3-carboxaldehyde, Heliyon. 7 (2021) 1–15. https://doi.org/10.1016/j.heliyon.2021.e07529.
20. E.R. Johnson, S. Keinan, P. Mori-Sánchez, J. Contreras-García, A.J. Cohen, W. Yang, Revealing noncovalent interactions, J. Am. Chem. Soc. 132 (2010) 6498–6506. https://doi.org/10.1021/ja100936w.
21. M.C. Sekhar, D. Wakgiri, D.N. Kenie, Study of Intermolecular Interactions between 2-Chloroaniline Isomeric Butanol Complexes in Gas Phase by Using DFT, NBO, QTAIM and RDG Analysis M.CHANDRA, Asian J. Chem. 31 (2019) 538–544. https://doi.org/10.14233/ajchem.2019.21651.
22. K. Vanasundari, V. Balachandran, M. Kavimani, B. Narayana, Molecular docking, vibrational, structural, electronic and optical studies of {4 – (2, 6) dichlorophenyl amino 2 – methylidene 4 – oxobutanoic acid and 4- (2, 5)} dichlorophenyl amino 2 – methylidene 4 – oxobutanoic acid – A comparative study, J. Mol. Struct. 1155 (2018) 21–38. https://doi.org/10.1016/j.molstruc.2017.11.002